A Firn Densification Process in the High Accumulation Dome of Southeastern Greenland

Authors: Iizuka, Yoshinori, Miyamoto, Atsushi, Hori, Akira, Matoba, Sumito, Furukawa, Ryoto, et al.

Source: Arctic, Antarctic, and Alpine Research, 49(1) : 13-27

Published By: Institute of Arctic and Alpine Research (INSTAAR), University of Colorado

URL: https://doi.org/10.1657/AAAR0016-034

Arctic, Antarctic, and Alpine Research, Vol. 49, No. 1, 2017, pp. 13–27
DOI: http://dx.doi.org/10.1657/AAAR0016-034

A firn densification process in the high accumulation dome of southeastern Greenland

Yoshinori Iizuka[1,*], Atsushi Miyamoto[2,*], Akira Hori[3], Sumito Matoba[1], Ryoto Furukawa[1], Takeshi Saito[1], Shuji Fujita[4], Motohiro Hirabayashi[4], Satoru Yamaguchi[5], Koji Fujita[6], and Nozomu Takeuchi[7]

[1]Institute of Low Temperature Science, Hokkaido University, Kita 19-jo Nishi 8-chome, Kita-ku, Sapporo, 060 0819, Japan
[2]Institute for the Advancement of Higher Education, Hokkaido University, Kita 17-jo Nishi 8-chome, Kita-ku, Sapporo, 060 0817, Japan
[3]Kitami Institute of Technology, 165 Koen-cho, Kitami, 090 8507, Japan
[4]National Institute of Polar Research, 10-3, Midori-cho, Tachikawa, 190 8518, Japan
[5]National Research Institute for Earth Science and Disaster Resilience, Suyoshi, Nagaoka, 940 0821, Japan
[6]Graduate School of Environmental Studies, Nagoya University, F3-1(200) Furo-cho, Chikusa-ku, Nagoya, 464 8601, Japan
[7]Department of Earth Sciences, Chiba University, 1-33, Yayoicho, Inageku, Chiba-city, Chiba, 263 8522, Japan
[*]Corresponding authors' email; iizuka@lowtem.hokudai.ac.jp (Iizuka), and miyamoto@lowtem.hokudai.ac.jp (Miyamoto)

A B S T R A C T

We examine a firn core from a dome in southeast Greenland that exhibits distinct firn densification. The ice was –20.9 °C at 20 m depth, and the core gives an average accumulation rate of 1.0 m w.e. yr^{-1} in water equivalent. However, the close-off density of 830 kg m^{-3} occurs at 83.4–86.8 m depth, which is about 20-m shallower than that obtained from two empirical models. Where the density $\rho > 750$ kg m^{-3}, the densification appears faster than that from the empirical models. As a result, compared to the empirical coefficient, the actual compactive viscosity coefficient is nonlinear and decreases at $\rho > 750$ kg m^{-3}, indicating that the firn with a higher density is softer than that from the empirical result. We argue here that the high accumulation rate creates a high overburden pressure in a short time. Thus, the relative softness of the firn may arise from (1) there being not enough time to form bonds between grains as strong as those in a lower accumulation-rate area, and similarly, (2) the dislocation density in the firn being relatively high.

Introduction

Polar ice sheets are good archives of paleoenvironmental events through the identification of proxies preserved in the ice. Such paleoenvironmental proxies are particularly well identified and dated in ice-sheet domes. Therefore, many ice cores have been drilled from ice sheet domes such as Dome Fuji (Watanabe et al., 2003), EPICA Dome C (EPICA community members, 2004), GRIP (Greenland Ice-Core Project Members, 1993), GISP2 (Grootes et al., 1993), and NGRIP (North Greenland Ice Core Project Members, 2004). Such domes often have common characteristics such as (1) a low accumulation rate, due to being in a polar inland area, and (2) a low temperature, due to being inland and at a relatively high elevation. Because the areas have low accumulation rates and low temperatures, the firn cores can provide reconstructions to past environments up to several hundred thousand years old. Moreover, as the areas experience limited melt, the measurements are of high quality. However, firn cores from areas with low accumulation rates have the disadvantages of low temporal resolution for the purpose of environmental reconstruction and might not track some seasonal or annual events (Kameda et al., 2008).

For paleoenvironmental reconstruction by gas proxy from ice cores, firn densification is an important factor. Firn densification is also a consideration for mass fluctuations of glaciers and ice sheets (Bader, 1939, 1958; Benson, 1962; Anderson and Benson, 1963), with the basic characteristics described in textbooks (e.g., Cuffey and Paterson, 2009). In inland Greenland, the transition from firn to ice typically occurs at a depth of 50 to 80 m and at ages of 100 to 300 years (e.g., Schwander et al., 1993; NEEM community members, 2013; Matoba et al., 2015). The main physical influences on firn densification are temperature, accumulation rate, and impurity levels. Concerning the impurities, impurity in firn accelerates deformation (densification) of firn, with Ca^{2+} (Hörhold et al., 2012) as well as Cl^{-}, NH_4^{2+}, F^{-} (Fujita et al., 2016) being key impurities for the deformation. Concerning temperature and accumulation rate, warm temperatures speed up the transition, but rapid accumulation increases the transition depth. In polar ice sheets, the high accumulation sites tend to be warm. This is probably because warm temperatures produce much more water vapor, which generally leads to greater precipitation rates. Thus, their temperature and accumulation have counteracting effects on the transition depth.

However, a recently studied dome area in southeast Greenland has one of the highest accumulation rates in Greenland yet is relatively cold, and thus may have novel firn characteristics. In a previous drilling project, we obtained a 90-m firn core in the southeast dome of Greenland (Iizuka et al., 2016). The site (67.18°N, 36.37°W, 3170 m a.s.l.) is located 185 km north of the town of Tasiilaq in southeastern Greenland. Hereafter; we call this site "SE-Dome." (This site is also called "Ammassalik Ice Cap" in Weidick and Morris, 1998, or it may be called "Dome Ammassalik.") The borehole temperature at a depth of 20 m was –20.9 °C. The main Greenland ice divide has a fork at the southern Summit (GRIP/GISP2). In the southern area of the fork, the two ice divides extend southwest to near Narsarsuaq through Dye 3, and extend southeast to near Tasiilaq. Likely due to the presence of a mountain under the ice sheet (Bamber et al., 2013) and to a high snow accumulation (Burgess et al., 2010), the SE-Dome area forms a dome more than 3000 m above sea level (Fig. 1).

According to Bales et al. (2009), the region has an accumulation rate of 0.6–0.8 m in water equivalent (w.e.), which is higher than that at other Greenland domes, due to a high moisture supply from the Icelandic low in the nearby Atlantic. Also, according to analysis of the DAS2 firn core (67.5°N, 36.1°W), the annual accumulation during the years from 1936 to 2002 was about 0.9 m (Pedro et al., 2012). Thus, a firn core from the SE-Dome will have the advantages of coming from the highest accumulation dome in Greenland and be of high quality due to the cold temperatures. To obtain comprehensive knowledge for firn densification, we should clarify the firn densification mechanism under conditions of a high accumulation rate.

In this study, we analyze a firn core in the SE-Dome region that extends below the close-off depth (Iizuka et al., 2016). Here we describe the core's physical characteristics, focusing on the firn densification process of the core as a case of high accumulation rate with low temperature.

Ice Core Processing and Analytical Procedures

The SE-Dome core (Fig. 1) was drilled to 90.45 m depth during 22–27 May 2015 and then transported by a 20-ft reefer ship from Tasiilaq, Greenland, to the Institute of Low Temperature Science (ILTS) at Hokkaido University, Japan, arriving on 24 August 2015 (Iizuka et al., 2016). During transit, the ice was kept below –25 °C. Upon arrival, we first confirmed that all firn-core sections were undamaged and had high quality. Then, we processed and analyzed the ice in the ILTS laboratory cold room.

For the analyses, we run stratigraphical observations and bulk density measurements on whole sections. Bulk density is measured with a volumetric method (measuring weight and size of the cores). A continuous density profile of the SE-Dome firn core is also measured using the X-ray transmission method reported by Hori et al. (1999). In this method, the intensity of X-rays transmitted through a firn core sample is continuously measured using an X-ray detector during translation of the sample across the beam. The X-ray intensity profile is then converted into a density profile using a calibration curve for X-ray absorption based on ice thickness. The spatial resolution of the density profile is approximately 1 mm. To detect volcanic events, and thus locate dates, we run electrical-conductivity measurements via the continuous dielectric profile (DEP) method (Fujita et al., 2016). This method produces a profile of electrical conductivity at 250 MHz. To detect the year 1963, the tritium content is determined using the liquid scintillation method after distilling the meltwater (Kamiyama et al., 1989). This method has an analytical resolution of 500 mm, which corresponds to about a half year.

According to a previous study, the ion concentrations in the surface snow are lower than those at other sites in inland Greenland (Iizuka et al., 2016; Oyabu et al., 2016). The reason is probably due to a dilution effect from the high accumulation. However, the ion fluxes are nearly the same as those in the GISP2 (Summit) snow

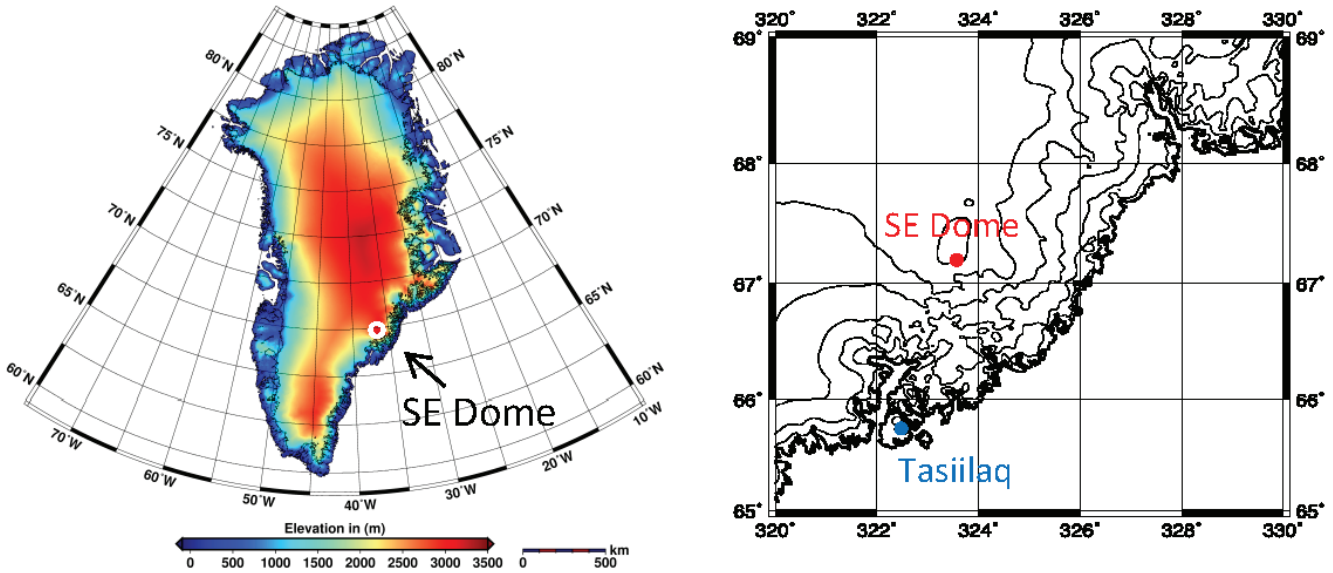

FIGURE 1. Location of SE Dome. Base of Greenland elevation map is from Helm et al. (2014). Right: close-up of study location. The core is from 67.18°N, 36.37°W, and 3170 m a.s.l.

(Oyabu et al., 2016), implying that the contribution of impurity to the firn deformation is smaller than that at other sites in Greenland. So, for this study, we do not account for impurity effects on firn deformation.

Results and Discussion

Stratigraphy and Density of Cores

The SE-Dome core consists of 189 sections, the average section length being 0.479 m. The bulk density of these sections increases with depth as plotted in Fig. 2, part a (See Table A1 for the raw values). At about the 13.8 m depth, the value 550 kg m^{-3} is reached, and then at about 20.2 m, the value reaches 600 kg m^{-3}. This density indicates the point where the firn grains stop rearranging (Fujita et al., 2014). Then at about 64.0 m depth, 760 kg m^{-3} is reached, meaning that below this depth, dislocation creep is a significant factor until close-off (Salamatin et al., 2009). Finally, at about 86.8 m, the close-off density of 830 kg m^{-3} is reached. These bulk densities agree well with the X-ray density measurements. For example, the X-ray close-off density is reached at 83.4 m. In comparison to other cores, the SE-Dome core has a relatively deep and young close-off depth (Fig. 3).

The observed number of ice layers equals 60, with an average thickness of 3.6 mm (Fig. 2, part a). Most of the ice layers are <5 mm thick, but several are much larger. For example, at 19.355 m depth (summer 2006), the ice layer is about 20 mm thick, and at depths of both 22.715 m (about 2004) and 86.490 m (about 1961) lie ice layers about 15 mm thick. Also, the 7.815 m depth has 7.1-mm ice layer, which is probably due to summer melting in 2012 (Nghiem et al., 2012). There is no ice layer at all near the surface after the ice layer in 2012, indicating cool summers around this region after 2013 to present. To determine the age of these depths, we count the density maxima and minima.

The profile of the X-ray density (Fig. 2, part b) has several peaks that exceed twice the standard deviation from a 2-m running average. These peaks indicate ice layers as described above. Indeed, depths having ice layers over 5 mm thick occur where there are X-ray density peaks. The standard deviation of the 2-m running mean is about 30 kg m^{-3} near the surface and decreases to 5 kg m^{-3} at 20 to 30 m depth (580 and 650 kg m^{-3}). In deeper firn, the standard deviation increases with depth to 15 kg m^{-3} at the close-off depth.

The minimum value of the standard deviation, here between 20 and 30 m (580 and 650 kg m^{-3}), in general marks the crossover point (Hörhold et al., 2011; Fujita et al., 2014, 2016). At this point, an initially low-density layer overtakes that of an initially high-density layer. Concerning season variations, wind forcing in winter in inland Greenland produces a homogeneous high-density surface snow (Benson, 1962). But during summer, insolation and temperature forcing after deposition produces a mixture of high- and low-density snow. So, the initially low-density layers come from summer precipitation, the high-density layers come from winter. As a reference, in this (southeastern) region, most precipitation falls during the winter months (Cappelen et al., 2001).

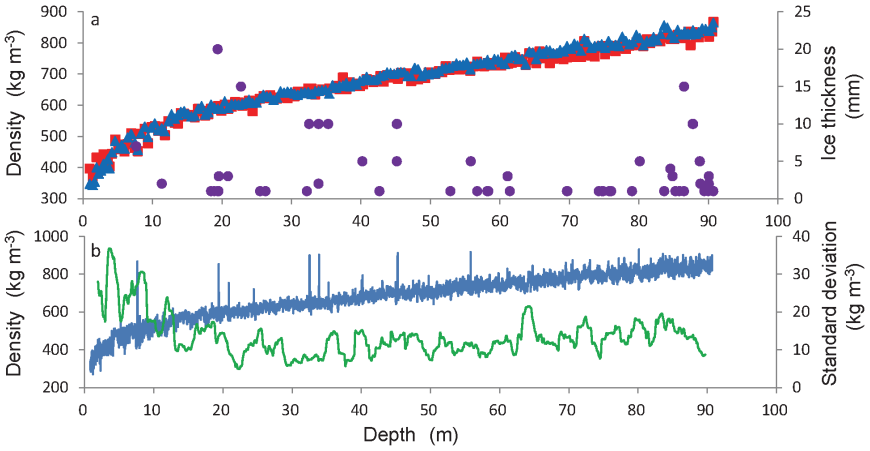

FIGURE 2. SE Dome firn-core profiles. (a) Bulk density (red squares), averaged x-ray density (blue triangles), and thickness of ice layers (purple circles). For the raw data of bulk and x-ray density, see Appendix, Table A1. (b) X-ray density (blue), and its standard deviation from the 2-m running average (green).

As the 2-m running-mean length roughly equals the annual accumulation, deviations probably reflect seasonal variation. Thus, the SE-Dome region has about 60 kg m^{-3} (1 σ) of seasonal density variation near the surface, which is smaller than the modeled one (about 200 kg m^{-3} under an accumulation rate of 0.9 m w.e. yr^{-1}; Li and Zwally, 2004).

Accumulation Rate of SE-Dome Firn Core

The smaller-scale density changes derive from the high-resolution X-ray density profile in Figure 4. The density fluctuates down to the 20-m depth with a period of 1 to 1.5 m, indicating initial winter high- and summer low-density layers. The fluctuations disappear from 20 to 30 m at the crossover point. Below the 30 m depth, the fluctuations reappear, probably due to having inverted summer high- and winter low-density layers.

Some conductivity peaks are detected (Fig. 4). The conductivity peak at 11.745 m depth is probably due to the eruption of the Eyjafjallajökull volcano from March to June 2010. In agreement with the eruption date, the 11.745 m depth corresponds to spring 2010 from counting maxima in the X-ray density profile (Fig. 4, part a). Moreover, according to the Volcanic Ash Advisory on the MET Office UK (http://www.metoffice.gov.uk/), volcanic materials were transported to southeastern Greenland at this time. Thus, using this date, the 11.745 m depth corresponds to 5.27 m in water equivalent, indicating an accumulation rate of 1.05 m w.e. yr^{-1} from spring 2010 to spring 2015.

The highest conductivity peak occurs at 43.420 m depth (Fig. 4, part b). The peak is probably due to the Pinatubo eruption on 15 June 1991. The 43.420 m depth corresponds to late autumn because the inverted density profiles correspond to a decreasing trend just before a minimum (Fig. 4, part b). This several-month time lag is likely due to the long distance for the eruption products to travel (Soden et al., 2002). The 43.420 m depth corresponds to 24.89 m in water equivalent, indicating an accumulation rate of 1.04 m w.e. yr^{-1} from autumn 1991 to spring 2015, and 1.08 m w.e. yr^{-1} from autumn 1992 to spring 2015..

Another fixed date is provided by the tritium profile in Fig. 4, part c. The tritium peak at 81.375–81.875 m depth corresponds to 1963, arising from fallout from hydrogen-bomb tests. The depth corresponds to 52.98–53.38 m in water equivalent, indicating an accumulation rate of 1.02–1.03 m w.e. yr^{-1} from 1963 to spring 2015.

These three comparisons between 1991 and 1963 indicate that the high-resolution X-ray density profile in Figure 4 preserves annual fluctuations. But due to the low-amplitude of the fluctuations near the crossover depth, this annual counting is not perfect. Nevertheless, the high accumulation rate may enable partial annual counting below the cross-over depth. Such counting indicates that the ice close-off occurs in 1962, meaning that 53 years is needed to close off.

In summary, the SE-Dome firn core has an accumulation rate of about 1.0 (1.02 to 1.08) m w.e. yr^{-1} with little decadal fluctuation. In the following discussion, the firn temperature and accumulation rate of the SE-Dome core are fixed at –20.9 °C and 1.0 m w.e. yr^{-1}.

Comparison with Firn Densification Model

Many physical-based models of firn densification have been proposed (e.g., Arthern and Wingham, 1998; Zwally and Li, 2002; Helsen et al., 2008; Salamatin et al., 2009); however, most require many physical parameters, and some do not match measured profiles (Cuffey and Paterson, 2009). Thus, instead we use empirical fittings.

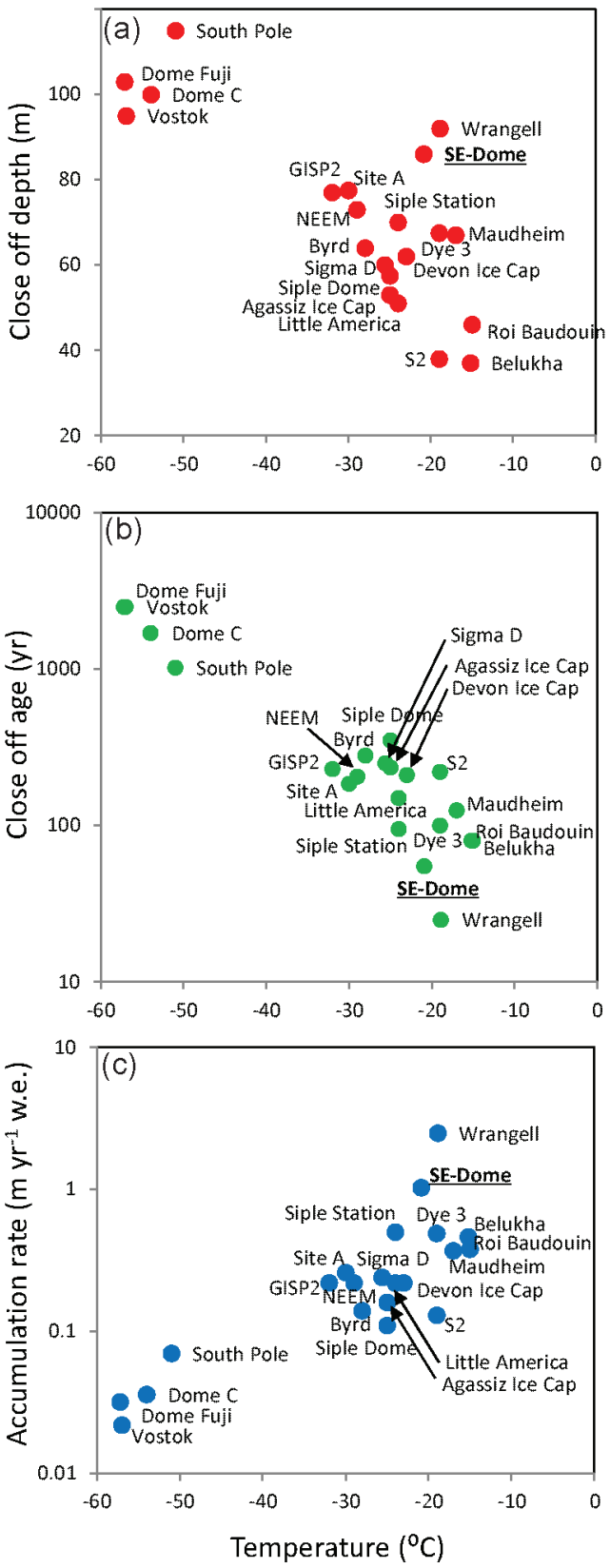

FIGURE 3. Characteristics of several firn cores with a range of temperatures and accumulation rates. (a) Relation of ice temperature with close-off depth. (b) Close-off age of ice. (c) Accumulation rate. For the raw data, see Table A2 in the Appendix.

For the polar high-elevation area, Sorge's Law (Sorge, 1935; Schytt, 1958) as well as Herron and Langway's model (Herron and Langway, 1980) are such fittings that match well with measured profiles of steady-state densification (Cuffey and Paterson, 2009). Fitting to Sorge's Law requires only the surface density (ρ_s), here 300 to 400 kg m^{-3}, and the close-off depth (h_c). The density (ρ_h) at any depth (h) is

$$\rho_h = \rho_i - [\rho_i - \rho_s]\exp\left(\frac{-h}{h_c / 1.9}\right) \quad (1)$$

As shown in Figure 5 (parts a–c), the depth-density curves derived from the parameter (h_c/1.9) match well with measured profiles in some regions in the polar high-elevation area. However, such a match does not occur with the SE-Dome firn core. Figure 6 shows several attempts to match this core to Sorge's Law. For both surface densities, the curves do not fit with the parameter (h_c/1.9 = 44.7 in the case h_c = 85 m). Instead, the h_c = 70% curve fits at $\rho < 550$ kg m^{-3}, and the h_c = 130% curve fits at $600 < \rho < 750$ kg m^{-3}. At $\rho < 550$ kg m^{-3}, the discrepancy may be related to the use of constant values of the surface density, with the DF and NEEM cores in Figure 5 showing a similar trend. However, unlike those other cores, at $600 < \rho < 750$ kg m^{-3}, the data do not fit with the h_c = 100% curve, instead fitting h_c = 130%. The 130% higher fitting suggests that the close-off depth should be about 108 m instead of the actual depth of 83.4–86.8 m.

Such a fit is similar to that found for the firn core drilled at Mount Wrangell, Alaska (Shiraiwa et al., 2004), a glacier with a high accumulation rate. That is, the depth-density curve of the Wrangell firn core shown in Fig. 5, part e, fits best when the parameter is 130% higher than hc/1.9. Both of these cores densify faster than Sorge's Law at densities $\rho > 750$ kg m^{-3}. In comparison, consider the ice from Mount Belukha, Russian Altai (Fig. 5, part d), which is mountain glacier in a high-elevation area with a normal accumulation rate. The depth-density curve of the Belukha firn core fits well with the parameter hc/1.9 (here 19.47 m). The features common to both SE-Dome and Wrangell are their high accumulation rates (1.03 and 2.49 m w.e. yr^{-1} w.e.) and younger close-off age (Fig. 3).

The depth-density curve does not match Herron and Langway's model well either. For the initial stage of densification ($\rho < 0.55$ kg m^{-3}), the density (ρ_h) at depth h is

$$\rho_h = \frac{\rho_i Z_0}{1 + Z_0}, \quad (2)$$

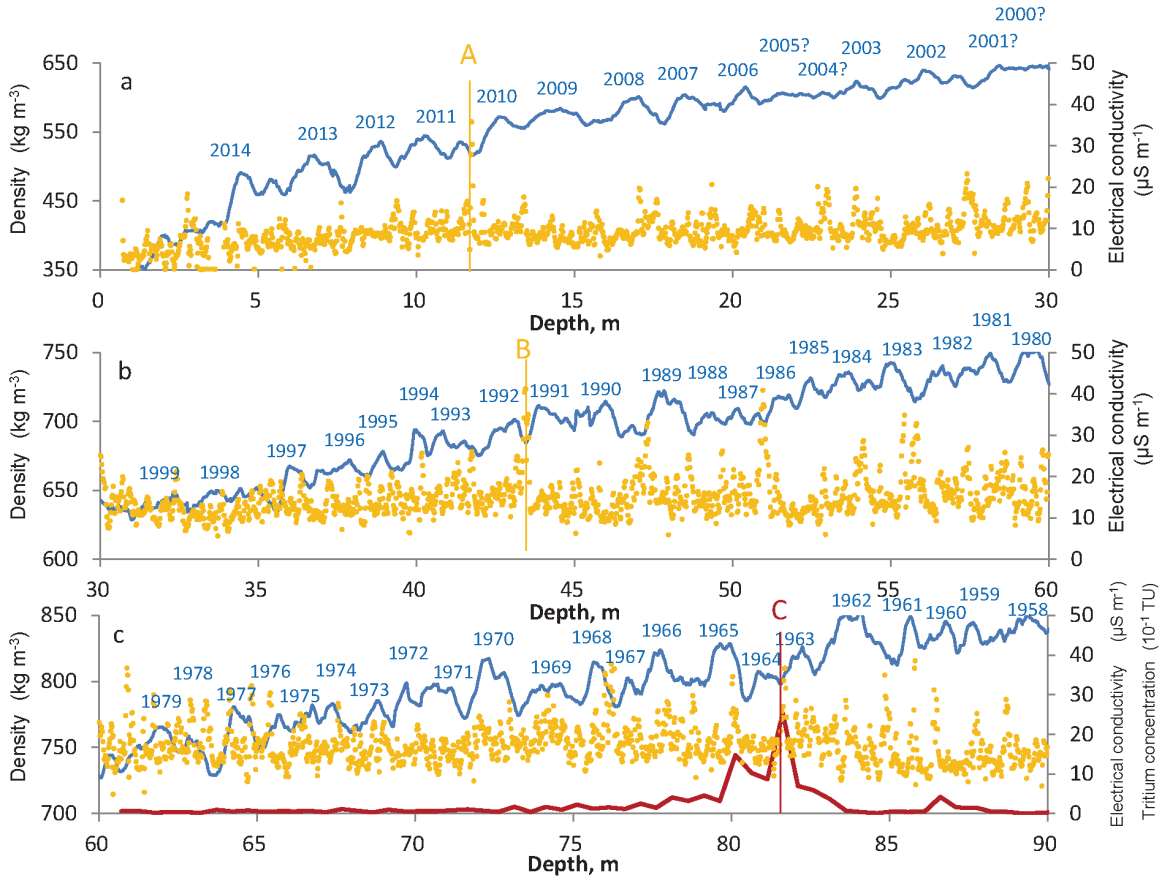

FIGURE 4. High-resolution x-ray density profile (blue), electrical conductivity (orange), and tritium concentrations (brown) of the SE Dome firn core. The density profile is a 40-mm running mean. The point marked A is the peak from the Eyjafjallajökull volcano on March to June 2010; B is the peak from the Pinatubo eruption on June 1991; C is the peak from nuclear tests in 1963.

where

$$Z_0 = \exp\left[\rho_i k_0 h + \ln\left(\frac{\rho_s}{\rho_i - \rho_s}\right)\right] \quad (3)$$

Here k_0 = 0.0862 at –20.9 °C.

For the following stage of densification (ρ > 0.55 kg m^{-3}), the density (ρ_h) at depth h is:

$$\rho_h = \frac{\rho_i Z_1}{1 + Z_1}, \quad (4)$$

where

$$Z_1 = \exp\left[\frac{\rho_i k_1 (h - h_{0.55})}{A^{0.5}} h + \ln\left(\frac{\rho_{0.55}}{\rho_i - \rho_{0.55}}\right)\right] \quad (5)$$

Here k_1 = 0.0211 at –20.9 °C, and the accumulation rate A = 1.0 m w.e. year^{-1}.

Figure 7 compares the measured profile to model results. At the initial stage of densification, when ρ < 0.55 kg m^{-3}, the depth-density curve matches the model's result for 0.36 kg m^{-3} of surface density. But at the following stage of densification, when ρ > 0.55 kg m^{-3}, the depth-density curve of the SE-Dome firn core does not match the model's result for 1 m w.e. yr^{-1} of annual accumulation. For this accumulation rate, the estimated close-off depth would be about 107–108 m in depth, the same value predicted from Sorge's Law and much deeper than the actual depth (from 83 to 86 m).

Firn Densification Mechanism in a High Accumulation Area

We consider here why the depth-density curve of SE-Dome firn core did not agree with the empirical models. In particular, we ask why the SE-Dome core densified faster at ρ > 750 kg m^{-3} than that predicted by Sorge's Law (Fig. 6). Figure 6 shows a good fit first to the H_c = 70% curve at ρ < 550 kg m^{-3} and then

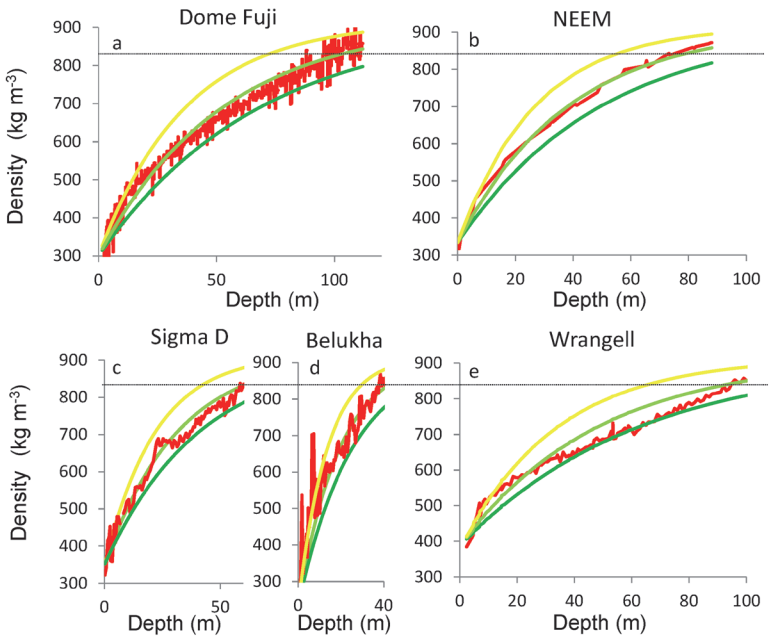

FIGURE 5. Comparison between measured density-depth profiles (red lines) with fits based on Sorge's Law. (a) Dome Fuji (Hondoh et al., 1999), (b) NEEM (Fujita et al., 2014), (c) SIGMA D (Matoba et al., 2015), (d) Belukha (Takeuchi et al., 2004), and (e) Wrangell (Shiraiwa et al., 2004). Light green curve is the fit using the parameter hc/1.9. Green and yellow curves are those using the parameter 1.3 times larger (130%) and 0.7 times larger (70%), respectively. The close-off depths hc are listed in Appendix Table A2.

to the H_c = 130% curve at 600 < ρ < 750 kg m^{-3}. But then the measured density increases faster than the 130% curve at ρ > 750 kg m^{-3}. Consider the compactive viscosity coefficient (η_c; Pa s^{-1}) in Figure 8, part a. The coefficient of the actual density profile is calculated from the equation

$$\eta_c = \sigma \cdot \rho \cdot \left(\frac{d\rho}{dt} \right)^{-1}, \qquad (6)$$

where, ρ, σ, and t are density (kg m^{-3}), overburden pressure (Pa), and time (s), respectively. On the other hand, the empirical compactive viscosity coefficient (η) with density dependence is calculated from the equation (Nishimura et al., 1983)

$$\eta = \eta_0 \cdot \exp(K \cdot \rho) \cdot \exp\left(\frac{\Delta E}{k_B T} \right), \qquad (7)$$

where, η_0 = 0.001 to 0.007 N*s m^{-2}, K = 2.57 × 10^{-3} m^3 kg^{-1}, ΔE is an activation energy equal to 51.6 kJ mol^{-1}, k_b is Boltzmann's constant, and T is the temperature. The empirical plot in density versus compactive viscosity coefficient in Figure 8, part a, shows a wide range of values because of a wide range of values for η_0. As a result, direct comparison is not possible between the empirical and the actual coefficients. However, the fit is linear in the linear-log plot at the lower densities. On the other hand, the actual compactive viscosity coefficient (η_c) is nonlinear (Fig. 8, part a), saturating at a fixed value when ρ >750 kg m^{-3}. The

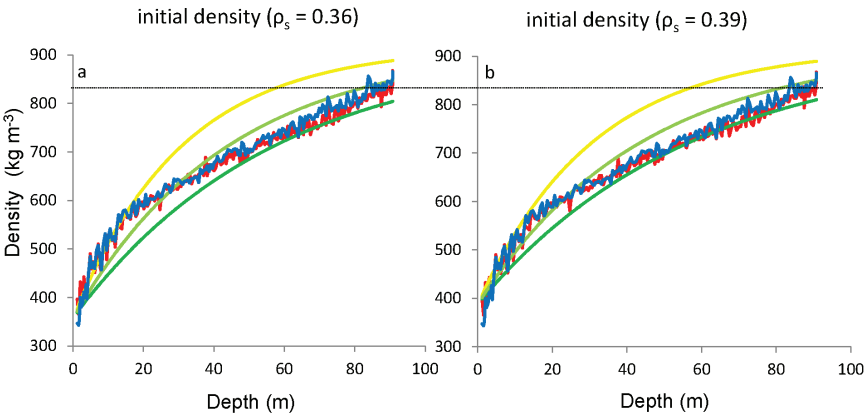

FIGURE 6. Same as Figure 5, but for the SE Dome firn core. Density-depth profiles are bulk (red) and x-ray (blue) measurements. (a) With initial density of 360 kg m^{-3}. (b) Initial density of 390 kg m^{-3}.

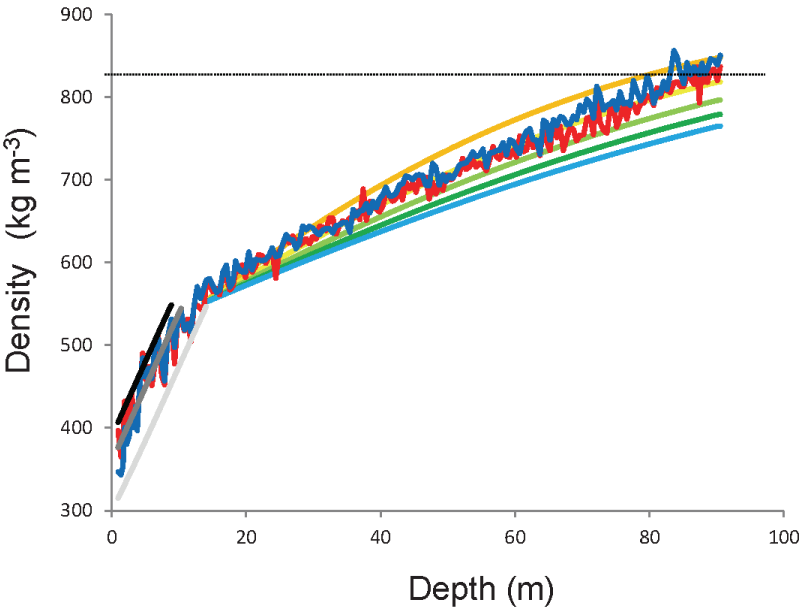

FIGURE 7. Same as Figure 6, but instead compared with the Herron and Langway (1980) model. Measured density-depth profiles are bulk (red line) and x-ray (blue) measurements. At the initial stage of the densification (ρ < 550 kg m^{-3}), black, dark gray, and light gray curves are model results for surface densities of 0.39, 0.36, and 0.30, respectively. In this model, the results are sensitive to accumulation rate only when ρ > 550 kg m^{-3}. Orange, yellow, light green, green, and light blue curves are model results for accumulation rates of 0.5, 0.75, 1.0, 1.25, and 1.5 m w.e. yr^{-1}, respectively. Model parameters are K_0 = 0.0862 and K_1 = 0.0211, with a temperature of –20.9 °C. Parameter $h_{0.55}$ is set to our measured value of 13.8 m.

lower compactive viscosity coefficient at ρ > 750 kg m^{-3} means that the SE-Dome firn at ρ > 750 kg m^{-3} is actually softer than the empirical relation predicts. This indicates that the SE-Dome firn is more deformable at ρ > 750 kg m^{-3}.

To better understand the densification, consider the relation of overburden pressure (Pa) to strain rate (m yr^{-1}). Comparing various sites, the SE-Dome core has a higher strain rate than other Greenland sites (SIGMA-D and NEEM cores) at a given overburden pressure (Fig. 8, part b). The difference is especially large, about one order of magnitude, at higher pressures (> 4 × 10^5 Pa; 750 kg m^{-3}). This indicates SE-Dome firn is more deformable at ρ >750 kg m^{-3} compared to that at other

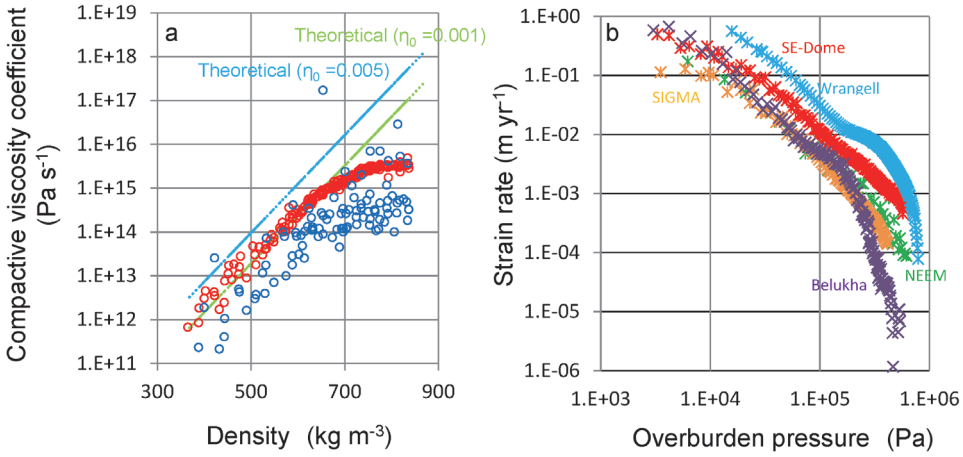

FIGURE 8. Inferred ice properties from the core. (a) Compactive viscosity coefficients (Pa s^{-1}). Blue and red circles are coefficients of bulk density from Equation (1) in the text. Blue circles are calculated from raw data. Red circles are calculated from a sixth-order polynomial approximation of the density-depth plot. As the raw data produces some negative coefficients because of density reversion between adjacent datapoints, the polynomial approximation is also used for the calculation. For the constants in the polynomial approximation, see Appendix, Table A3. Light green (η_0 = 0.001) and blue lines (η_0 = 0.005) are empirical coefficients from Equation (2) in the text. (b) The relation between overburden pressure (Pa) and strain rate (m yr^{-1}) of several firn cores; SE Dome (red), NEEM (green), SIGMA D (orange), Belukha (purple), and Wrangell (light blue). Polynomial approximation of the density profiles is used for the calculation. For the constant numbers of polynomial approximation, see Appendix, Table A3.

Greenland sites. The Wrangell core has an even higher strain rate than the SE-Dome core. As the Wrangell core has about 2.5 times the accumulation rate of the SE-Dome core, the Wrangell firn may be more deformable than SE-Dome firn. On the other hand, Belukha firn is less deformable than SE-Dome firn. Of the five cores plotted in Fig. 8, part b, Belukha firn has the highest ice temperature, indicating that this relation of overburden pressure (Pa) and strain rate (m yr^{-1}) does not depend on the ice temperature. Rather, accumulation rate is one of the key factors that determines the strain rate for a given overburden pressure.

We have two possible reasons why the SE-Dome firn is more deformable at $\rho > 750$ kg m^{-3} than prediction. First, the SE-Dome region has one of the highest accumulation rate areas in polar ice domes (Fig. 3). A high accumulation rate creates a high overburden pressure in a short time. The short time leads to a weaker bond strength between grains than that of the same depth in a lower accumulation rate area. This condition makes it easier to deform (densify) the snow/firn than that of the same depth in a lower (or normal) accumulation rate area. In other words, firn in high accumulation rate areas are predisposed toward a high overburden pressure at $\rho > 750$ kg m^{-3} without fully bonded growth, resulting in a more rapid densification than that in the empirical steady-state condition. The second possible reason is that, dislocation creep is a significant process in densification at $\rho > 750$ kg m^{-3} (Salamatin et al., 2009). As a high accumulation rate creates a high overload pressure in a short time, the dislocation density is likely to increase in firn in a shorter time than that in firn with a normal accumulation rate. Thus, the SE-Dome core may have faster densification at $\rho > 750$ kg m^{-3} than the depth-density curve with a normal accumulation rate.

Conclusion

We have shown that the core from SE-Dome in Greenland has a distinct firn-densification profile due to the area's high accumulation rate. Probably because of the high accumulation rate, the SE-Dome firn core preserved its annual fluctuation even after the cross-over point and caused the depth-density curve to deviate from Sorge's Law and the Herron and Langway model. Concerning the latter, the modeled close-off depth (108 m) is over 20 m deeper than the actual depth (from 83.4 to 86.8 m).

The actual compactive viscosity coefficient was nonlinear, particularly at $\rho > 750$ kg m^{-3}, indicating that the SE-Dome firn at $\rho > 750$ kg m^{-3} is softer than that from empirical plots. Among firn cores from other areas, both of the high-accumulation cores (SE-Dome and Wrangell) tend to be more deformable (high strain rate) at the same overburden pressure than that from the models. We offered two hypotheses for this greater deformability at $\rho > 750$ kg m^{-3}. The high accumulation rate creates a high overburden pressure in a short time. The short timing has two effects: Compared to firn in a lower accumulation-rate area, here (1) there is not enough time to form strong bonds between grains, and (2) the dislocation density is likely to be higher.

Acknowledgments

We are grateful to the drilling team of SE-Dome ice. The paper was significantly improved as a result of comments by two anonymous referees and the handling by Scientific Editor Dr. A. Jennings, to whom we are greatly indebted. This study was supported by MEXT/JSPS KAKENHI Grant Number 26257201 and 16K12573, Joint Research Program of the Institute of Low Temperature Science, Hokkaido University, and the Readership program of the Institute of Low Temperature Science, Hokkaido University. The analysis of tritium concentration was supported by National Institute of Polar Research through General Collaboration Project no. 27-13. This study is partly responsible for ArCS (Arctic Challenge for Sustainability Project; PI Shin Sugiyama)

References Cited

Anderson, D. L., and Benson, C. S., 1963: The densification and diagenesis of snow. *In* Kingery, W. D. (ed.), *Ice and snow: properties, processes, and applications*. Cambridge, Massachusetts: MIT Press, 391–411.

Arthern, R. J., and Wingham, D. J., 1998: The natural fluctuations of firn densification and their effect on the geodetic determination of ice sheet mass balance. *Climatic Change*, 40(4): 605–624.

Bader, H., 1939: Mineralogische und strukturelle Charakterisierung des Schnees und seiner Metamorphose. *In* Bader, H., and 6 others (eds.), *Der Schnee und seine Metamorphose*. Beiträge zur Geologie der Schweiz, Geotechnische Serie Hydrologie 3, 1–61 [Transl. Tienhaven, J. C. V., 1954: Snow and its metamorphism, *SIPRE Translations*, 14: 1–55].

Bader, H., 1958: Sorge's law of densification of snow of high polar glaciers. *Journal of Glaciology*, 2(15): 319–323.

Bales, R. C., Guo, Q., Shen, D., McConnell, J. R., Du, G., Burkhart, J. F., Spikes, V. B., Hanna, E., and Cappelen, J., 2009: Annual accumulation for Greenland updated

using ice core data developed during 2000–2006 and analysis of daily coastal meteorological data. *Journal of Geophysical Research*, 114: D06116, doi http://dx.doi.org/10.1029/2008JD011208.

Bamber, J. L., Griggs, J. A., Hurkmans, R. T. W. L., Dowdeswell, J. A., Gogineni, S. P., Howat, I., Mouginot, J., Paden, J., Palmer, S., Rignot, E., and Steinhage, D., 2013: A new bed elevation data-set for Greenland. *The Cryosphere*, 7: 499–510, doi http://dx.doi.org/10.5194/tc-7-499-2013.

Benson, C. S., 1962: Stratigraphic studies in the snow and firn of the Greenland ice sheet. *SIPRE Research Report*, 70: 76–83.

Burgess, E. W., Forster, R. R., Box, J. E., Mosley-Thompson, E., Bromwich, D. H., Bales, R. C., and Smith, L. C., 2010: A spatially calibrated model of annual accumulation rate on the Greenland Ice Sheet (1958–2007). *Journal of Geophysical Research*, 115: F02004, doi http://dx.doi.org/10.1029/2009JF001293.

Cappelen, J., Jørgense, B.V., Laursen, E.V., Stannius, L. S., and Thomsen, R. S., 2001: *The Observed Climate of Greenland, 1958–99—with climatological standard normals, 1961–90*. Danish Meteorological Institute Technical Report 00-18.

Cuffey, K. M., and Paterson, W. S. B., 2009: *The Physics of Glaciers*. 4th edition. Oxford, U.K.: Butterworth-Heinemann.

EPICA community members, 2004: Eight glacial cycles from an Antarctic ice core. *Nature*, 429: 623–628, doi http://dx.doi.org/10.1038/nature02599.

Fujita, S., Hirabayashi, M., Goto-Azuma, K., Dallmayr, R., Satow, K., Zheng, J., and Dahl-Jensen, D., 2014: Densification of layered firn of the ice sheet at NEEM, Greenland. *Journal of Glaciology*, 60(223): 905–921, doi: http://dx.doi.org/10.3189/2014JoG14J006.

Fujita, S., Goto-Azuma, K., Hirabayashi, M., Hori, A., Iizuka, Y., Motizuki, Y., Motoyama, H., and Takahashi, K., 2016: Densification of layered firn in the ice sheet at Dome Fuji, Antarctica. *Journal of Glaciology*, 62(231): 103–123, doi http://dx.doi.org/10.1017/jog.2016.16.

Greenland Ice-core Project Members, 1993: Climate instability during the last interglacial period recorded in the GRIP ice core. *Nature*, 364: 203−207.

Grootes, P. M., Stuiver, M., White, J. W. C., Johnsen, S., and Jouzel, J., 1993: Comparison of oxygen isotope records from the GISP2 and GRIP Greenland ice cores. *Nature*, 366: 552–554, doi http://dx.doi.org/10.1038/366552a0.

Helm, V., Humbert, A., and Miller, H., 2014: Elevation and elevation change of Greenland and Antarctica derived from CryoSat-2. *The Cryosphere*, 8: 1539–1559, doi http://dx.doi.org/10.5194/tc-8-1539-2014.

Helsen, M. M., van den Broeke, M. R., van de Wal, R. S. W., van de Berg, W. J., van Meijgaard, E., Davis, C. H., Li, Y., and Goodwin, I., 2008: Elevation changes in Antarctica mainly determined by accumulation variability. *Science*, 320: doi http://dx.doi.org/10.1126/science.1153894.

Herron, M. M., and Langway, C. C., 1980: Firn densification: an empirical model. *Journal of Glaciology*, 25(93): 373–385.

Hondoh, T., Narita, H., Hori, A., Fujii, M., Shoji, H., Kameda, T., Mae, S., Fujita, S., Ikeda, T., Fukazawa, H., Fukumura, T., Azuma, N., Wong, Y., Kawada, K., Watanabe, O., and Motoyama, H., 1999: Basic analyses of Dome Fuji deep ice core, part 2: physical properties. *Polar Meteorology and Glaciology,* 13: 90–98.

Hörhold, M. W., Kipfstuhl, S., Wilhelms, F., Freitag, J., and Frenzel, A., 2011: The densification of layered polar firn. *Journal of Geophysical Research*, 116(F1): F01001, doi: http://dx.doi.org/10.1029/2009JF001630.

Hörhold, M. W., Laepple, T., Freitag, J., Bigler, M., Fischer, H., and Kipfstuhl, S., 2012: On the impact of impurities on the densification of polar firn. *Earth and Planetary Science Letters*, 325: 93–99, doi http://dx.doi.org/10.1016/j.epsl.2011.12.022.

Hori, A., Tayuki, K., Narita, H., Hondoh, T., Fujita, S., Kameda, T., Shoji, H., Azuma, N., Kamiyama, K., Fujii, Y., Motoyama, H., and Watanabe, O., 1999: A detailed density profile of the Dome Fuji (Antarctica) shallow ice core by X-ray transmission method. *Annals of Glaciology*, 29: 211–214.

Iizuka, Y., Matoba, S., Yamasaki, T., Oyabu, I., Kadota, M., and Aoki, T., 2016: Glaciological and meteorological observations at the SE-Dome site, southeastern Greenland Ice Sheet. *Bulletin of Glaciological Research*, 34: 1–10: doi http://dx.doi.org/10.5331/bgr.15R03.

Kameda, T., Motoyama, H., Fujita, S., and Takahashi, S., 2008: Temporal and spatial variability of surface mass balance at Dome Fuji, East Antarctica, by the stake method from 1995 to 2006. *Journal of Glaciology*, 54: 107–116, doi http://dx.doi.org/10.3189/002214308784409062.

Kamiyama, K., Ageta, Y., and Fujii, Y., 1989: Atmospheric and depositional environments traced from unique chemical compositions of the snow over an inland high plateau, Antarctica. *Journal of Geophysical Research*, 94(D15): 18515–18519.

Li, J., and Zwally, H. J., 2004: Modeling the density variation in shallow firn layer. *Annals of Glaciology*, 38: 309–313.

Matoba, T., Motoyama, H., Fujita, K., Yamasaki, T., Minowa, M., Onuma, Y., Komuro, Y., Aoki, T., Yamaguchi, S., Sugiyama, S., and Enomoto, H., 2015, Glaciological and meteorological observations at the SIGMA-D site, northwestern Greenland Ice Sheet. *Bulletin of Glaciological Research,* 33: 7–14, doi http://dx.doi.org/10.5331/bgr.33.7.

NEEM community members, 2013: Eemian interglacial reconstructed from a Greenland folded ice core. *Nature*, 493: 489–494, doi http://dx.doi.org/10.1038/nature11789.

Nghiem, S. V., Hall, D. K., Mote, T. L., Tedesco, M., Albert, M. R., Keegan, K., Shuman, C. A., DiGirolamo, N. E., and Neumann, G., 2012:The extreme melt across the Greenland Ice Sheet in 2012. *Geophysical Research Letters*, 39: L20502, doi http://dx.doi.org/10.1029/2012GL053611.

Nishimura, H, Maeno, N., and Satow, K., 1983: Snow structure and depth hoar formation in Mizuho Plateau, Antarctica. *Memoirs of National Institute of Polar Research*, 29: 149–158.

North Greenland Ice Core Project Members, 2004: High-resolution record of northern hemisphere climate extending into the last interglacial period. *Nature*, 431: 147–151, doi http://dx.doi.org/10.1038/nature02805.

Okamoto, S., Fujita, K., Narita, H., Uetake, J., Takeuchi, N., Miyake, T., Nakazawa, F., Aizen, V. B., Nikitin, S. A., and Nakawo, M., 2011: Reevaluation of the reconstruction of summer temperatures from melt features in Belukha ice cores, Siberian Altai. *Journal of Geophysical Research*, 116: D02110, doi http://dx.doi.org/10.1029/2010JD013977.

Oyabu, I., Matoba, S., Yamasaki, T., Kadota, M.Y., and Iizuka, Y., 2016: Seasonal variations in the major chemical species of snow at the South East Dome in Greenland. *Polar Science*, doi http://dx.doi.org/10.1016/j.polar.2016.01.003.

Pedro, J. B., McConnell, J. R., van Ommen, T. D., Fink, D., Curran, M. A. J., Smith, A. M., Simon, K. J., Moy, A. D., and Das, S. B., 2012: Solar and climate influences on ice core ^{10}Be records from Antarctica and Greenland during the neutron monitor era. *Earth and Planetary Science Letters*, 355–356: 174–186, doi http://dx.doi.org/10.1016/j.epsl.2012.08.038.

Salamatin, A. N., Lipenkov, V.Y., Barnola, J. M., Hori, A., Duval, P., and Hondoh, T., 2009: Snow/firn densification in polar ice sheets. *In* Hondoh, T. (ed.), *Institute of Low Temperature Science, Special Issue*, 68: 195–222.

Schwander, J., Banola, J.-M., Andrié, C., Leuenberger, M., Ludin, A., Raynaud, D., and Stauffer, B., 1993: The age of the air in the firn and the ice at Summit, Greenland. *Journal of Geophysical Research,* 98: 2831–2838.

Schytt, V., 1958: Glaciology II. A: Snow studies at Maudheim. Glaciology. B: Snow studies inland. Glaciology. C: The inner structure of the ice shelf at Maudheim as shown by core drilling. Norwegian-British-Swedish Antarctic Expedition, 1949–52. *Scientific Results*, Volume 4.

Shiraiwa, T., Kanamori, S., Benson, C. S., Solie, D., and Muravyev, Y. D., 2004: Shallow ice-core drilling at Mount Wrangell, Alaska. *Bulletin of Glaciological Research*, 21: 71–78.

Soden, B. J., Wetherald, R. T., Stenchikov, G. L., and Robock, A., 2002: Global cooling after the eruption of Mount Pinatubo: a test of climate feedback by water vapor. *Science*, 296(5568):727–730, doi http://dx.doi.org/10.1126/science.296.5568.727.

Sorge, E., 1935: Glaziologische Untersuchungen in Eismitte. *In* Brockamp, B., Jülg, H., Loewe, F., and Sorge, E. (eds.), *Wissenschaftliche Ergebnisse der Deutschen GrönLand-Expedition Alfred Wegener 1929 und 1930/1931. Band III. Glaziologie*. Leipzig, Germany: F. A. Brockhaus, 62–270.

Takeuchi, N., Takahashi, A., Uetake, J., Yamazaki, Y., Aizen, V., Joswiak, D., Surazakov, A., and Nikitin, S., 2004: A report on ice core drilling on the western plateau of Mt. Belukha in the Altai Mountain Range in 2003. *Polar Meteorology and Glaciology*, 18: 121–133.

Watanabe, O., Jouzel, J., Johnsen, S., Parrenin, F., Shoji, H., and Yoshida, N., 2003: Homogeneous climate variability across East Antarctica over the past three glacial cycles. *Nature*, 422(6931): 509–512, doi http://dx.doi.org/10.1038/nature01525.

Weidick, A., and Morris, E., 1998: Local glaciers surrounding the continental ice sheets. *In* Haeberli, W., Hoelzle, M., and Suter, S. (eds.), *Into the Second Century of World Glacier Monitoring—Prospects and Strategies*. Paris: UNESCO Studies and Reports in Hydrology, 56, 167–176.

Zwally, H. J., and Li, J., 2002: Seasonal and interannual variations of firn densification and ice-sheet surface elevation at Greenland summit. *Journal of Glaciology*, 48(161): 199–207.

MS submitted 10 May 2016
MS accepted 28 September 2016

Appendix

TABLE A1

Depth and density data of each core section as shown in Figure 2, part a.

Core No.	Top(m)	Bottom (m)	Bulk density (kg m^{-3})	X-ray density (kg m^{-3})	Core No.	Top (m)	Bottom (m)	Bulk density (kg m^{-3})	X-ray density (kg m^{-3})	Core No.	Top (m)	Bottom (m)	Bulk density (kg m^{-3})	X-ray density (kg m^{-3})
SE-001	0.690	1.185	397	347	SE-064	29.670	30.175	631	642	SE-127	60.955	61.445	734	750
SE-002	1.185	1.565	365	343	SE-065	30.175	30.655	629	637	SE-128	61.445	61.945	736	759
SE-003	1.565	1.805	388	354	SE-066	30.655	31.155	644	633	SE-129	61.945	62.435	754	762
SE-004	1.805	2.075	432	400	SE-067	31.155	31.655	643	639	SE-130	62.435	62.935	739	749
SE-005	2.075	2.355	389	380	SE-068	31.655	32.140	639	641	SE-131	62.935	63.465	747	748
SE-006	2.355	2.805	400	389	SE-069	32.140	32.645	654	641	SE-132	63.465	63.965	729	731
SE-007	2.805	3.075	443	411	SE-070	32.645	33.135	654	636	SE-133	63.965	64.465	767	772
SE-008	3.075	3.430	421	400	SE-071	33.135	33.645	634	645	SE-134	64.465	64.975	746	769
SE-009	3.430	3.680	422	426	SE-072	33.645	34.145	645	645	SE-135	64.975	65.445	736	748
SE-010	3.680	3.925	403	397	SE-073	34.145	34.635	650	648	SE-136	65.445	65.955	772	773
SE-011	3.925	4.355	444	449	SE-074	34.635	35.145	647	649	SE-137	65.955	66.465	751	766
SE-012	4.355	4.875	490	485	SE-075	35.145	35.700	654	637	SE-138	66.465	66.935	765	776
SE-013	4.875	5.310	459	461	SE-076	35.700	36.135	654	664	SE-139	66.935	67.425	736	775
SE-014	5.310	5.755	474	472	SE-077	36.135	36.645	662	656	SE-140	67.425	67.935	750	767
SE-015	5.755	6.160	451	460	SE-078	36.645	37.155	652	662	SE-141	67.935	68.435	764	768
SE-016	6.160	6.670	475	496	SE-079	37.155	37.645	689	663	SE-142	68.435	68.905	761	777
SE-017	6.670	7.180	510	507	SE-080	37.645	38.135	651	671	SE-143	68.905	69.375	747	773
SE-018	7.180	7.685	464	480	SE-081	38.135	38.635	674	660	SE-144	69.375	69.935	754	790
SE-019	7.685	8.060	452	457	SE-082	38.635	39.125	669	674	SE-145	69.935	70.485	755	782
SE-020	8.060	8.595	508	509	SE-083	39.125	39.605	665	666	SE-146	70.485	70.905	775	797
SE-021	8.595	9.125	525	532	SE-084	39.605	40.075	661	677	SE-147	70.905	71.435	776	792
SE-022	9.125	9.575	478	497	SE-085	40.075	40.560	668	682	SE-148	71.435	71.885	755	775
SE-023	9.575	10.075	530	528	SE-086	40.560	41.050	684	691	SE-149	71.885	72.385	806	813
SE-024	10.075	10.565	533	542	SE-087	41.050	41.540	681	681	SE-150	72.385	72.875	770	803
SE-025	10.565	11.065	517	519	SE-088	41.540	42.040	674	681	SE-151	72.875	73.405	760	785
SE-026	11.065	11.570	532	526	SE-089	42.040	42.530	677	684	SE-152	73.405	73.895	757	790
SE-027	11.570	11.975	504	516	SE-090	42.530	43.010	693	694	SE-153	73.895	74.375	785	792
SE-028	11.975	12.525	549	548	SE-091	43.010	43.510	676	696	SE-154	74.375	74.890	790	796
SE-029	12.525	12.935	548	571	SE-092	43.510	44.010	697	705	SE-155	74.890	75.360	764	785
SE-030	12.935	13.485	544	557	SE-093	44.010	44.500	689	703	SE-156	75.360	75.870	775	806
SE-031	13.485	13.845	541	568	SE-094	44.500	45.050	696	700	SE-157	75.870	76.370	790	792

Continued

TABLE A1

Core No.	Top(m)	Bottom (m)	Bulk density (kg m^{-3})	X-ray density (kg m^{-3})	Core No.	Top (m)	Bottom (m)	Bulk density (kg m^{-3})	X-ray density (kg m^{-3})	Core No.	Top (m)	Bottom (m)	Bulk density (kg m^{-3})	X-ray density (kg m^{-3})
SE-032	13.845	14.295	575	579	SE-095	45.050	45.500	685	705	SE-158	76.370	76.900	773	794
SE-033	14.295	14.800	573	581	SE-096	45.500	45.980	703	706	SE-159	76.900	77.360	792	790
SE-034	14.800	15.350	565	572	SE-097	45.980	46.480	694	706	SE-160	77.360	77.880	791	820
SE-035	15.350	15.830	569	564	SE-098	46.480	46.960	703	694	SE-161	77.880	78.380	781	806
SE-036	15.830	16.300	561	566	SE-099	46.960	47.470	677	693	SE-162	78.380	78.890	792	796
SE-037	16.300	16.805	588	589	SE-100	47.470	47.980	697	720	SE-163	78.890	79.390	793	802
SE-038	16.805	17.300	581	597	SE-101	47.980	48.450	683	715	SE-164	79.390	79.880	802	826
SE-039	17.300	17.850	567	570	SE-102	48.450	48.980	693	693	SE-165	79.880	80.375	800	815
SE-040	17.850	18.200	572	576	SE-103	48.980	49.510	687	706	SE-166	80.375	80.900	790	793
SE-041	18.200	18.645	588	602	SE-104	49.510	49.990	706	698	SE-167	80.900	81.375	811	806
SE-042	18.645	19.160	590	592	SE-105	49.990	50.460	700	705	SE-168	81.375	81.875	800	804
SE-043	19.160	19.655	597	589	SE-106	50.460	50.955	701	702	SE-169	81.875	82.335	812	819
SE-044	19.655	20.150	582	588	SE-107	50.955	51.445	709	709	SE-170	82.335	82.845	808	809
SE-045	20.150	20.635	602	613	SE-108	51.445	51.955	707	718	SE-171	82.845	83.375	806	828
SE-046	20.635	21.135	589	591	SE-109	51.955	52.445	726	720	SE-172	83.375	83.865	817	856
SE-047	21.135	21.640	595	604	SE-110	52.445	52.945	713	721	SE-173	83.865	84.355	819	849
SE-048	21.640	22.130	610	603	SE-111	52.945	53.460	715	726	SE-174	84.355	84.855	813	827
SE-049	22.130	22.640	608	602	SE-112	53.460	53.985	725	734	SE-175	84.855	85.325	813	816
SE-050	22.640	23.185	599	604	SE-113	53.985	54.470	715	728	SE-176	85.325	85.845	826	842
SE-051	23.185	23.620	607	608	SE-114	54.470	54.960	720	730	SE-177	85.845	86.380	822	827
SE-052	23.620	24.135	615	618	SE-115	54.960	55.490	717	737	SE-178	86.380	86.840	816	837
SE-053	24.135	24.675	581	607	SE-116	55.490	55.990	711	715	SE-179	86.840	87.330	837	830
SE-054	24.675	25.170	614	609	SE-117	55.990	56.470	725	732	SE-180	87.330	87.520	793	827
SE-055	25.170	25.700	621	622	SE-118	56.470	56.980	740	733	SE-181	87.520	88.060	834	841
SE-056	25.700	26.215	630	634	SE-119	56.980	57.470	728	735	SE-182	88.060	88.370	818	828
SE-057	26.215	26.675	624	628	SE-120	57.470	57.950	725	736	SE-183	88.370	88.860	818	834
SE-058	26.675	27.180	632	628	SE-121	57.950	58.480	735	745	SE-184	88.860	89.350	832	846
SE-059	27.180	27.665	625	617	SE-122	58.480	58.965	728	730	SE-185	89.350	89.850	834	845
SE-060	27.665	28.150	621	624	SE-123	58.965	59.455	727	748	SE-186	89.850	90.350	820	839
SE-061	28.150	28.680	624	644	SE-124	59.455	59.955	735	746	SE-187	90.350	90.720	837	851
SE-062	28.680	29.170	629	640	SE-125	59.955	60.455	728	738	SE-188	90.720	90.740	868	865
SE-063	29.170	29.670	623	644	SE-126	60.455	60.955	753	732	SE-189	90.740	90.815	no data	no data

TABLE A2

Temperature, accumulation rate, close-off depth, and age of several firn cores.

Location	Temperature (°C)	Accumulation rate (m w.e. yr^{-1})	Close off depth (m)	Age (yr)	References
Vostok	–57	0.02	95	2500	
Dome C	–54	0.04	100	1700	
South Pole	–51	0.07	115	1020	
GISP2	–32	0.22	77	230	
Site A	–30	0.26	75-80	185	
Byrd	–28	0.14	64	280	
Agassiz Ice Cap	–25	0.16	53	235	
Siple Dome	–25	0.11	55-60	350	
Little America	–24	0.22	51	150	
Siple Station	–24	0.50	70	95	
Devon Ice Cap	–23	0.22	62	210	
Dye 3	–19	0.49	65-70	100	
S2	–19	0.13	38	220	
Maudheim	–17	0.37	67	125	Table 2.2 in Cuffey and Paterson (2009)
Roi Baudouin	–15	0.38	46	80	
NEEM	–29	0.22	73	205	NEEM Community Members (2013)
Sigma D	–26	0.24	60	250	Matoba et al. (2015)
Dome Fuji	–57	0.03	103	2500	Hondoh et al. (1999)
Wrangell	–19	2.49	92	25	Shiraiwa et al. (2004)
Belukha	–15	0.46	37	80	Okamoto et al. (2011)
SE-Dome	–21	1.03	86(83)	55(53)	this study

TABLE A3

Parameters (A–G) of the sixth-order polynomial approximation in Figure 8. For Dp (depth [m]) and Dn (density [kg m^{-3}]), $Dn = A\,Dp^6 + B\,Dp^5 + C\,Dp^4 + D\,Dp^3 + E\,Dp^2 + F\,Dp + G$.

Constant numbers	A	B	C	D	E	F	G
NEEM	-1.09516×10^{-8}	3.69324×10^{-6}	-4.86931×10^{-4}	3.16700×10^{-2}	-1.09765×10^{0}	2.55220×10^{1}	3.20293×10^{2}
Sigma D	8.26461×10^{-10}	-2.47016×10^{-8}	-4.64240×10^{-5}	7.66437×10^{-3}	5.14490×10^{-1}	2.09032×10^{1}	3.48100×10^{2}
Wrangell	-3.67812×10^{-9}	1.52591×10^{-6}	-2.53374×10^{-4}	2.12772×10^{-2}	-9.38475×10^{-1}	2.35890×10^{1}	3.54737×10^{2}
Belukha	-2.01010×10^{-7}	4.84494×10^{-5}	-4.50820×10^{-3}	2.02846×10^{-1}	-4.61446×10^{-0}	5.91657×10^{1}	2.80979×10^{2}
SE-Dome	-6.95769×10^{-9}	2.43919×10^{-6}	-3.39102×10^{-4}	2.41679×10^{-2}	-9.50116×10^{-1}	2.33235×10^{1}	3.58420×10^{2}